Electronic Supplementary Information

Simultaneous atomic absorption and emission spectrometer with dielectric barrier discharge for atomization and excitation

Tao Lin,[a] Jing Hu,[b] Yujia Deng,[c] Wen Zeng,[b] Jiadeng Chen,[b] Xiaoming Jiang, *[b] and Xiandeng Hou,*[a,b]

[a]*Key Laboratory of Green Chemistry & Technology of MOE, College of Chemistry, Sichuan University, Chengdu, Sichuan 610064, China.*

[b]*Analytical & Testing Center, Sichuan University, Chengdu, Sichuan 610064, China.*

[c]*College of Chemistry and Chemical Engineering, China West Normal University, Sichuan 637001, China.*

Corresponding authors' E-mails: houxd@scu.edu.cn；jiangxm@scu.edu.cn

1. Details about the DBD microplasma

The DBD microplasma was sustained in a quartz tube (1.5 mm i.d., 3 mm o.d., and 70 mm length) and copper wire was wrapped tightly around the tube with a distance of 20 mm from each other. Volatile species were transferred into the plasma through a branch tube approximately 20 mm from one of the electrodes. The photographs of the quartz tube used for the construction of DBD microplasma and the Ar DBD microplasma at working state were shown in Fig. S1.

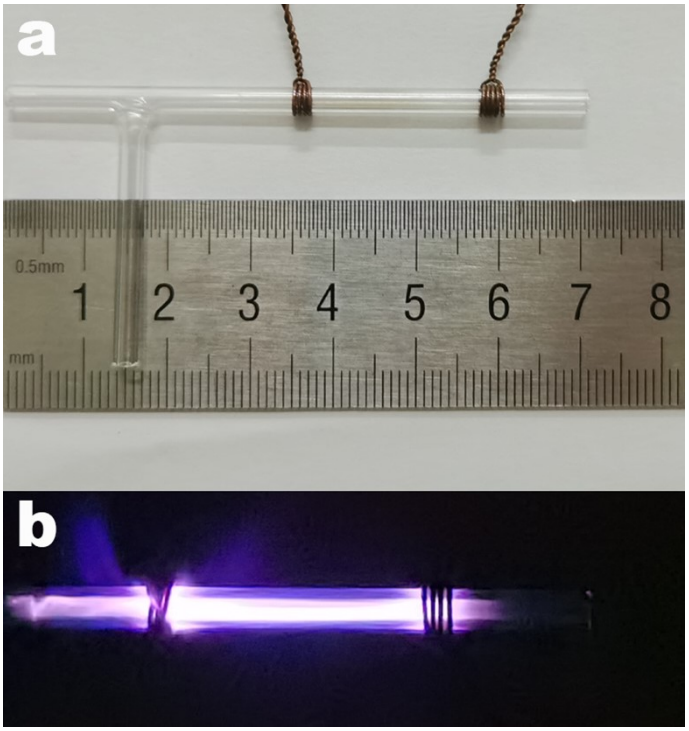

Fig. S1 Photographs of (a) quartz tube used for the construction of DBD microplasma, and (b) DBD microplasma at working state with Ar as the working gas.

2. Characterization of plasma physical parameters

2.1 Rotational temperature measurement

The rotational temperature T_{rot} of the OH molecules was determined on the basis of the unresolved rotational structure of the transition $A^2\Sigma^+$, v'=0 → $X^2\Pi$, v''=0 with rotational spectra fall in the range of 306-312 nm. The experimental molecular spectra were fitted with the simulated rotational lines at different T_{rot} values simulated by the LIFBASE software and then the T_{rot} corresponding to the experimental spectra was obtained. This approach was similar to that reported by Bruggeman et al.,[1] Swiderski et al.,[2] and Yuan et al.[3] Fig. S2 shows the calculation of T_{rot} of pure Ar capillary DBD plasma by LIFBASE and it can be seen that simulated spectra at a T_{rot} value of 450 K match well with the experimental data with a peak correlation value of 0.958 (Chi-square: 61.0); and the values of peak correlation for all simulated spectra of OH are better than 0.90.

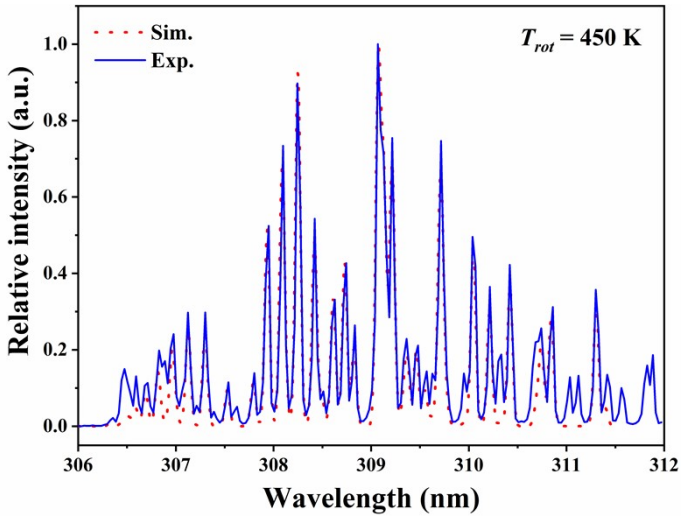

Fig. S2 Comparison between the experimental and simulated spectra of OH ($A^2\Sigma^+$-$X^2\Pi$, 306-312 nm) for calculating rotational temperature.

2.2 Excitation temperature measurement by using Boltzmann plot method

Based on the atomic emission spectra of Ar and He, respectively, the excitation temperature of the DBD plasma was obtained using the Boltzmann plot method[4, 5] shown in Eq. S1. The relevant parameters of the spectral lines of Ar and He used for temperature measurement were shown in Table S1, and the data was obtained from the NIST database.[6] Fig. S3 showed an example of the calculation of excitation temperature by the Boltzmann plot method of Ar (a) and He (b) emission spectra, respectively.

$$\lg\left(\frac{I\lambda}{gA}\right) = -\frac{5040 * E}{T} + C \qquad \text{(Eq. S1)}$$

Table S1 Information of relevant parameters of atomic spectral lines used for excitation temperature measurement.[6]

Wavelength (λ,	Excitation energy (*E*, cm⁻	*gA* (×10⁸ s⁻¹)
Ar		
706.72	107290	0.190
738.40	107290	0.425
763.51	106237	1.225
794.82	107132	0.558
800.62	106237	0.245
He		
492.19	191446	0.993
501.57	186209	0.401
587.56	186101	0.884
667.82	186105	3.185
706.52	184865	0.464

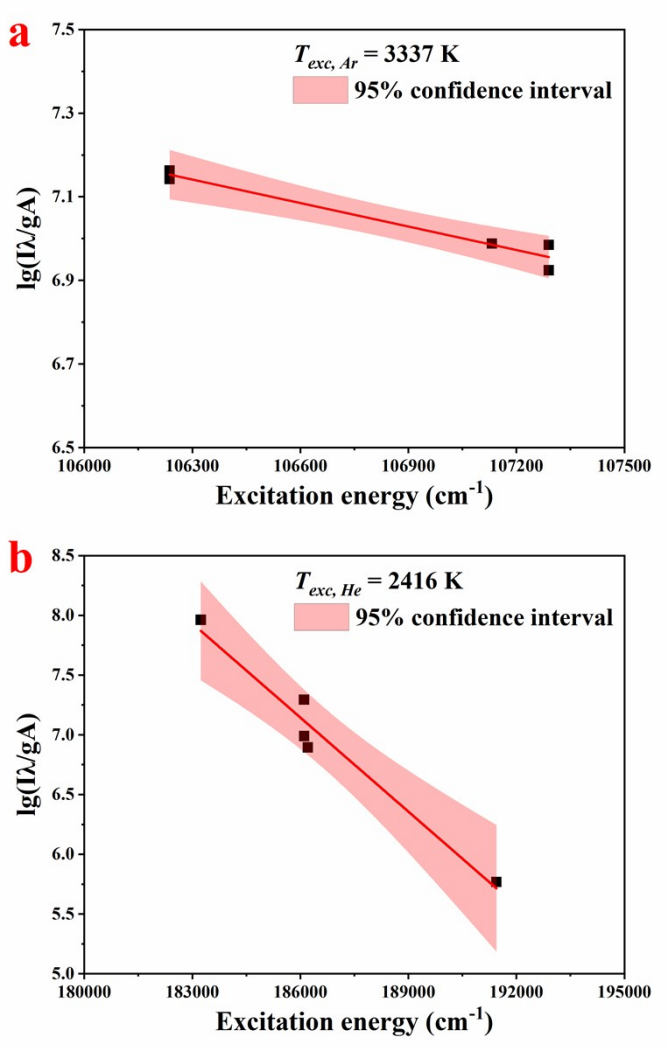

Fig. S3 Boltzmann plot of lg(*Iλ* / *gA*) *vs E* for excitation temperature of Ar (a) and He (b).

2.3 Electron density of capillary dielectric barrier discharges

The electron density n_e was calculated from the Stark broadening of H_β (486.1 nm) based on the following principle:[7, 8]

$$n_e = 10^{17} \times (\frac{\Delta\lambda_S}{4.8})^{1.46808} \ (\mathrm{cm}^{-3}) \qquad \text{(Eq. S2)}$$

where $\Delta\lambda_S$ is the full width at half maximum (FWHM) of Stark broadening of H_β in nm. The line width of H_β is mainly consisted of the Lorentzian broadening ($\Delta\lambda_L$) and Gaussian broadening ($\Delta\lambda_G$), which can be subdivided into Doppler broadening ($\Delta\lambda_D$), van der Waals broadening ($\Delta\lambda_{vdW}$), instrumental broadening ($\Delta\lambda_I$) and Stark broadening ($\Delta\lambda_S$).[3, 9, 10] For atmosphere pressure discharge, $\Delta\lambda_D$ and $\Delta\lambda_{vdW}$ are written approximately as:

$$\Delta\lambda_D = 3.48 \times 10^{-4} (T_g)^{1/2} \ (\mathrm{nm}) \qquad \text{(Eq. S3)}$$

$$\Delta\lambda_{vdW} = 5.16 (T_g)^{-7/10} \ (\mathrm{nm}) \qquad \text{(Eq. S4)}$$

The spectral line profile simulated by MATLAB software was compared with the experimental one to obtain the best fitting value and then calculate the electron density of the discharge plasma, as shown in Fig. S4. The electron density of the plasma was around the order of 10^{14} cm^{-3}.

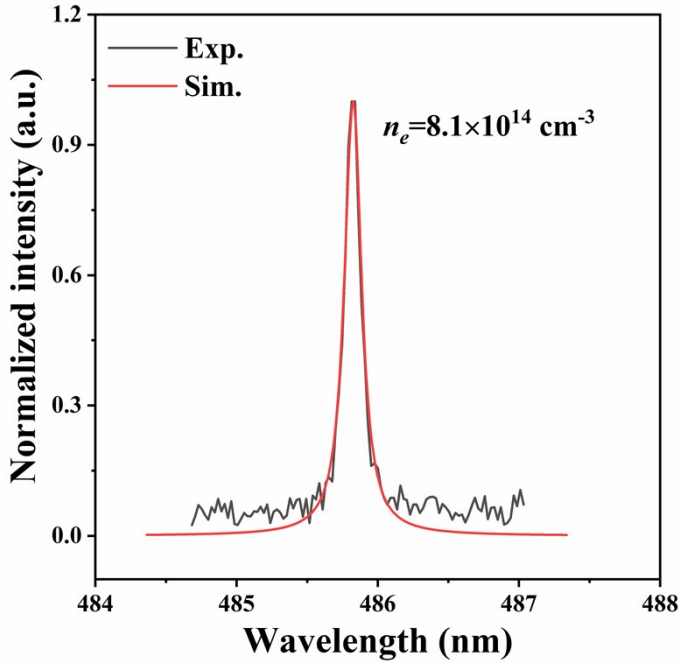

Fig. S4 Comparison between experimental and simulated spectra of H_β (486.1 nm) for electron density calculation.

2.4 Plasma physical properties

The values of physical parameters obtained through the above-mentioned emission spectroscopy were

illustrated in Fig. S5. The rotational temperature for all these plasmas were varied between 450-550 K. As for the excitation temperature, the values obtained from Ar Boltzmann plot were higher than that of He, and this is similar to those reported in the literatures.[11, 12] Electron densities of Ar and He plasmas were all up to the level of 10^{14} cm^{-3}, and these are similar to those of other inert gas microplasmas.[13, 14] As shown in Fig. S5, the doped gases showed a significant effect on the plasmas' excitation temperature and electron density, especially for the Ar discharge plasmas.

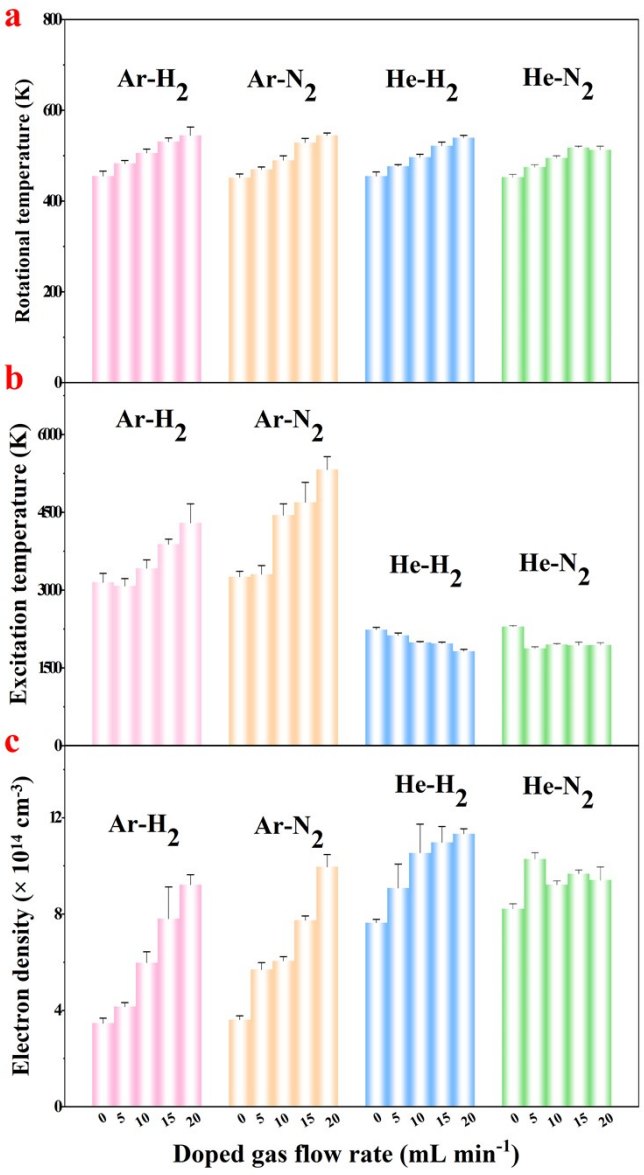

Fig. S5. Influence of doped gas on the plasma's physical property including (a) rotational temperature, (b) excitation temperature and (c) electron density.

3. Photos of plasma with different supporting gases at working state

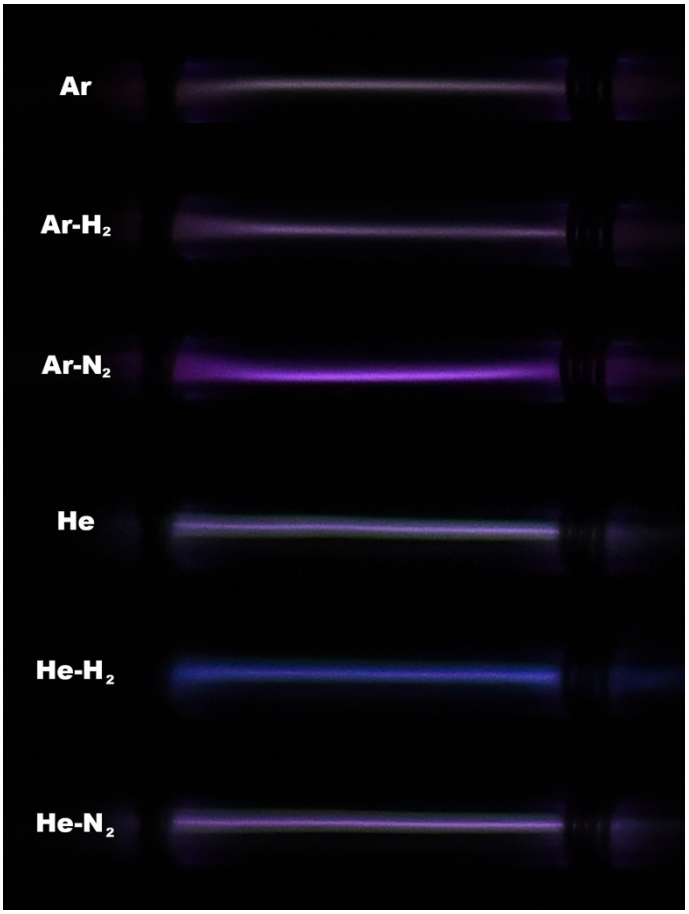

Fig. S6 Photos of plasmas with different supporting gases at working state.

4. Log-log calibration plots of AAS and AES responses in different gas discharges with chemical vapor generation as the sampling method

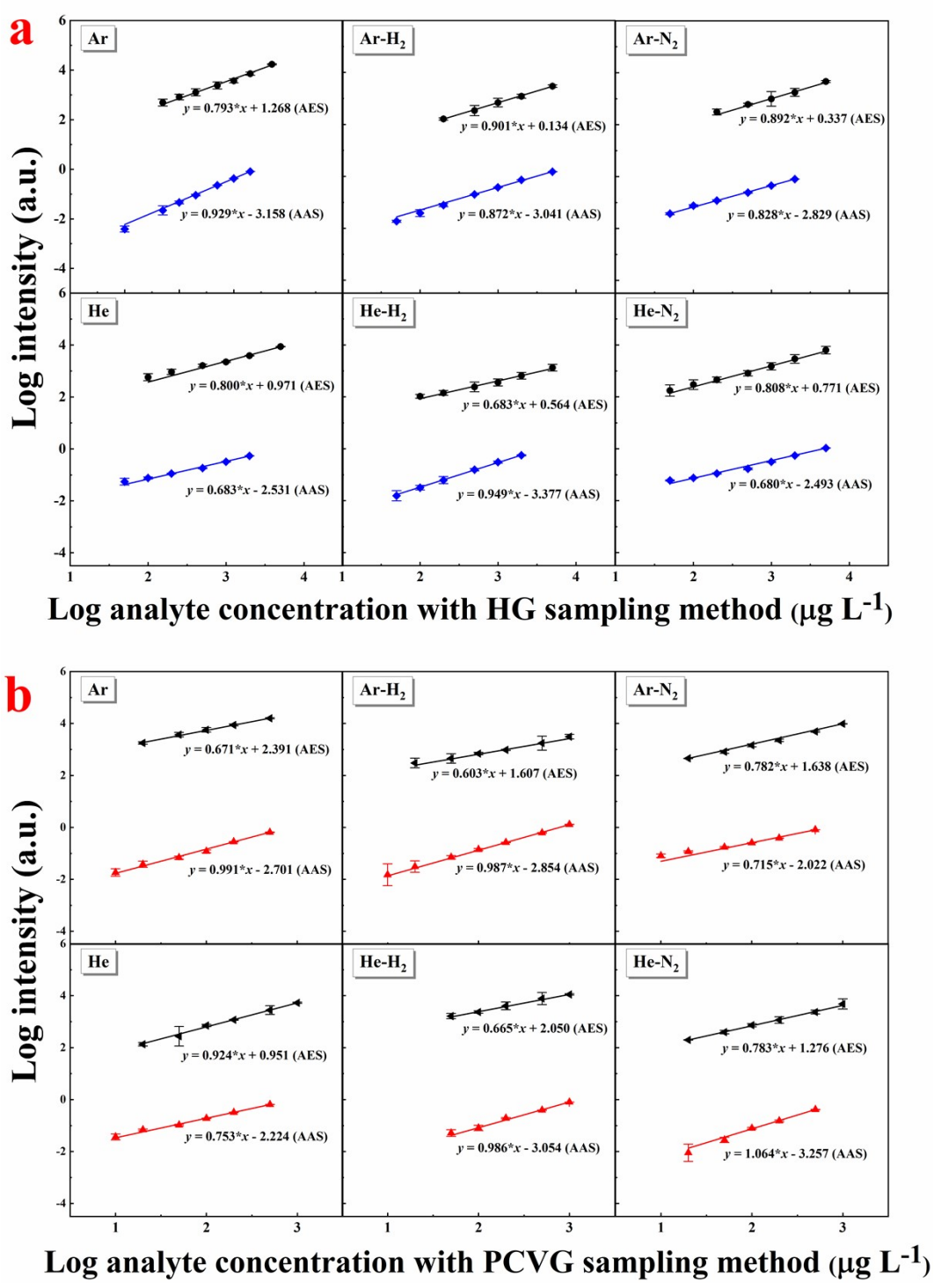

Fig. S7 Log-log calibration curves for AAS and AES signals of Hg in plasmas as a function of analyte concentration with different chemical vapor generation, HG (a) or PCVG (b), for sample introduction.

5. Analytical performance with hydride generation

The analytical performance of this AAS/AES simultaneous detection system with different supporting gases was preliminarily evaluated with hydride generation as the sampling method. The linear calibration relationships between AAS or AES response and concentration of Hg were presented in Fig. S8 and Fig. S9, respectively. The limit of detection (LOD) was calculated from 3 times of the standard deviation of 11 measurements of a blank solution divided by the slope of the calibration curve. The LODs of 0.005, 0.020, 0.014, 0.025, 0.030 and 0.013 μg mL^{-1} were obtained from the atomic absorption signals of different support gases, including Ar, Ar-H_2, Ar-N_2, He, He-H_2 and He-N_2, respectively. The LODs obtained through the atomic emission signals of different support gases including Ar-H_2, Ar-N_2, He, He-H_2 and He-N_2 were 0.020, 0.072, 0.026, 0.025, 0.094 and 0.026 μg mL^{-1}, respectively. Although the LODs obtained by AES are generally much higher than those obtained by AAS, the upper limit of AES's linear dynamic range is also higher than that of AAS, and this means that the combination of those two types of signals can broaden the linear dynamic range.[15]

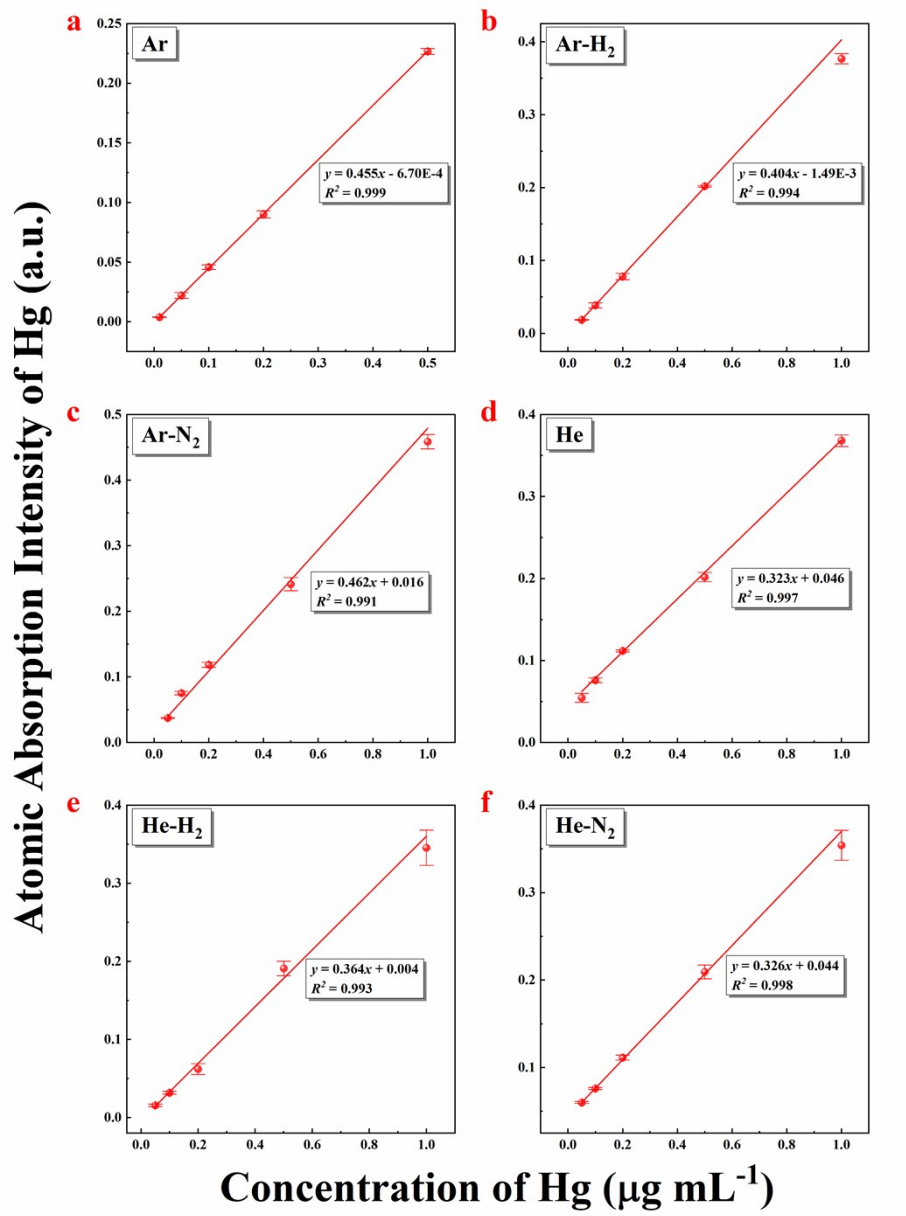

Fig. S8 The linear calibration relationships between AAS response obtained from plasmas with difference discharge gases and concentration of Hg with a hydride generation system.

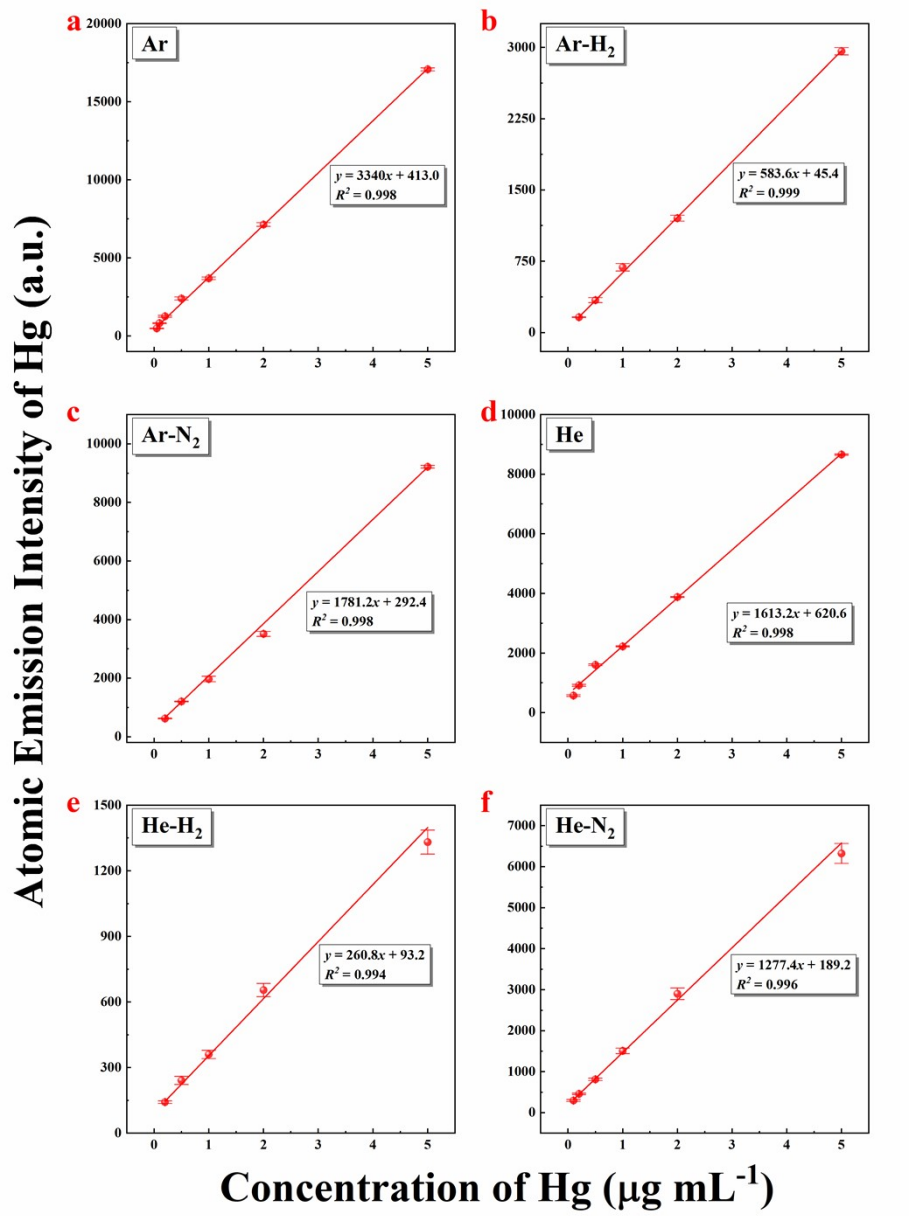

Fig. S9 The linear calibration relationships between AES response obtained from plasmas with difference discharge gases and concentration of Hg with a hydride generation system.

References

1. P. Bruggeman, E. Ribežl, A. Maslani, J. Degroote, A. Malesevic, R. Rego, J. Vierendeels and C. Leys, *Plasma Sources Sci. Technol.*, 2008, **17**, 025012.

2. K. Swiderski, A. Dzimitrowicz, P. Jamroz and P. Pohl, *J. Anal. At. Spectrom.*, 2018, **33**, 437-451.

3. H. Yuan, J. Feng, D. Z. Yang, X. F. Zhou, J. P. Liang, L. Zhang, Z. L. Zhao and W. C. Wang, *J. Appl. Phys.*, 2020, **128**, 9.

4. M. Li, K. Li, L. He, X. Zeng, X. Wu, X. Hou and X. Jiang, *Anal. Chem.*, 2019, **91**, 7001-7006.

5. P. Li, J. Hu, M. Zhang, L. He, K. Li, X. Hou and X. Jiang, *Anal. Chem.*, 2022, DOI: 10.1021/acs.analchem.2c01105.

6. A. Kramida, Ralchenko, Yu., Reader, J. and NIST ASD Team, NIST Atomic Spectra Database (version 5.8), https://physics.nist.gov/asd, DOI: https://doi.org/10.18434/T4W30F).

7. S. Yatom, Y. Luo, Q. Xiong and P. J. Bruggeman, *J. Phys. D: Appl. Phys.*, 2017, **50**, 415204.

8. V. Horvatic, S. Müller, D. Veza, C. Vadla and J. Franzke, *J. Anal. At. Spectrom.*, 2014, **29**, 498-505.

9. S. Djurović and N. Konjević, *Plasma Sources Sci. Technol.*, 2009, **18**, 035011.

10. S. Z. Li, C. J. Chen, X. Zhang, J. Zhang and Y. X. Wang, *Plasma Sources Sci. Technol.*, 2015, **24**, 025003.

11. E. Desjardins, M. Laurent, A. Durocher-Jean, G. Laroche, N. Gherardi, N. Naudé, L. Stafford, *Plasma Sources Sci. Technol.*, 2018, **27**, 015015.

12. R. K. Gangwar, O. Levasseur, N. Naudé, N. Ghérardi, F. Massines, J. Margot, L. Stafford, *Plasma Sources Sci. Technol.*, 2015, **25**, 015011.

13. B. Eliasson, U. Kogelschatz, IEEE T. on plasma science, 1991, **19**, 309-323.

14. T. Krähling, S. Geisler, M. Okruss, S. Florek, J. Franzke, *Spectrochim. Acta, Part B*, 2015, **114**, 20-26.

15. D. R. Jenke and R. Woodriff, *Appl. Spectrosc.*, 1982, **36**, 686-689.